WATER RESOURCES RESEARCH, VOL. 33, NO. 5, PAGES 935–945, MAY 1997

Beach water table fluctuations due to wave run-up: Capillarity effects

L. Li,[1] D. A. Barry, J.-Y. Parlange,[2] and C. B. Pattiaratchi

Department of Environmental Engineering, University of Western Australia, Nedlands, Western Australia

Abstract. High-frequency beach water table fluctuations due to wave run-up and run-down have been observed in the field [*Waddell*, 1976]. Such fluctuations affect the infiltration/exfiltration process across the beach face and the interstitial oxygenation process in the beach ecosystem. Accurate representation of high-frequency water table fluctuations is of importance in the modeling of (1) the interaction between seawater and groundwater, more important, the effects on swash sediment transport and (2) the biological activities in the beach ecosystem. Capillarity effects provide a mechanism for high-frequency water table fluctuations. Previous modeling approaches adopted the assumption of saturated flow only and failed to predict the propagation of high-frequency fluctuations in the aquifer. In this paper we develop a modified kinematic boundary condition (kbc) for the water table which incorporates capillarity effects. The application of this kbc in a boundary element model enables the simulation of high-frequency water table fluctuations due to wave run-up. Numerical tests were carried out for a rectangular domain with small-amplitude oscillations; the behavior of water table responses was found to be similar to that predicted by an analytical solution based on the one-dimensional Boussinesq equation. The model was also applied to simulate the water table response to wave run-up on a sloping beach. The results showed similar features of water table fluctuations observed in the field. In particular, these fluctuations are standing wave-like with the amplitude becoming increasingly damped inland. We conclude that the modified kbc presented here is a reasonable approximation of capillarity effects on beach water table fluctuations. However, further model validation is necessary before the model can confidently be used to simulate high-frequency water table fluctuations due to wave run-up.

1. Introduction

Coastal aquifers have a dynamic seaward boundary at the beach face where the observed physical processes (e.g., the pressure fluctuations) are influenced by oceanic water level fluctuations. Field observations show that the beach water table fluctuates in response to these sea level oscillations. Such interactions between seawater and coastal groundwater are important in at least two respects. First, the elevation of the beach water table significantly affects swash sediment transport and hence beach stability [e.g., *Grant*, 1948; *Duncan*, 1964]. A high beach water table tends to cause beach erosion, while a low water table promotes beach accretion [*Grant*, 1948]. Second, beach water table fluctuations may have a large impact on interstitial oxygenation processes and control to some extent the biological activity in the beach ecosystem [*McLachlan*, 1989]. It is therefore important to understand how sea level oscillations propagate into the aquifer.

Most previous research has been focused on low-frequency fluctuations of the groundwater table due to, for example, the tide [e.g., *Lanyon et al.*, 1982; *Nielsen*, 1990; *Li et al.*, 1996]. High-frequency water table oscillations due to wave run-up and run-down (swash/backwash; called only run-up hereinafter), however, have received little attention. *Waddell* [1976] carried out field measurements of high-frequency water table fluctuations. Direct measurements of the elevation of the beach water table landward of the swash zone were made, using capacitance probes. The results clearly demonstrate that the water table fluctuates in response to wave run-up. The periods of these fluctuations ranged from 8 to 20 s, which were well correlated to those of wave motion. More recently, *Hegge and Masselink* [1991] conducted a field study of beach water table interaction with swash at the Western Australian coast. They also used capacitance probes to measure the water table elevations and found similar water table responses.

Despite the field observations of high-frequency water table oscillations, many researchers have chosen to ignore them while simulating the fluctuations of the beach water table. Most existing models, including those based on the one-dimensional Boussinesq equation [e.g., *Nielsen*, 1990] and those solving the two-dimensional flow equation [e.g., *Li et al.*, 1996], consider only saturated flow. These models predict that the amplitude of the fluctuations is damped inland and that the damping rate increases with the frequency of the sea level oscillations [e.g., *Parlange et al.*, 1984]. Therefore, according to these models, high-frequency sea level oscillations do not induce water table fluctuations in coastal aquifers to any appreciable distance inland, a result which contradicts field observations. The absence of high-frequency water table fluctuations may lead to inaccurate simulation of the water infiltration/exfiltration across the beach face and the interstitial oxygen-

[1] Now at School of Engineering and Technology, Deakin University, Geelong, Victoria, Australia.

[2] Permanently at Department of Agricultural and Biological Engineering, Cornell University, Ithaca, New York.

Paper number 96WR03946.
0043-1397/97/96WR-03946$09.00

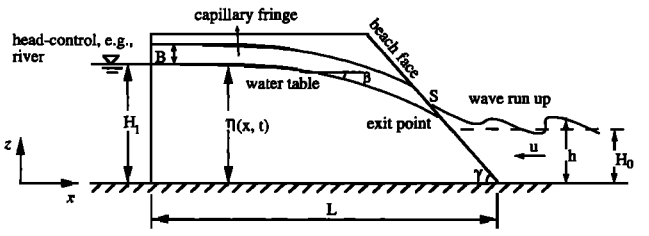

Figure 1. Schematic diagram of a coastal aquifer interacting with wave motion. (Inside the capillary fringe, water saturation is close to unity, and pressure is less than the atmospheric, i.e., capillary, pressure, the value of which is related to the water table elevation as $P = -\rho g(z - \eta)$.)

ation beneath the beach. The former process affects beach stability, and the latter plays an important role in the beach ecosystem.

Capillarity effects provide a mechanism for the propagation inland of high-frequency sea level oscillations. The existence of a capillary fringe above the beach water table has been confirmed by field measurements [e.g., *Turner*, 1993]. As the water table fluctuates, the pressure distribution above the water table will change, and thus an apparent local water exchange across the water table occurs. To incorporate this mass transfer process in the one-dimensional Boussinesq equation, *Parlange and Brutsaert* [1987] suggested an additional term be added to the Boussinesq equation. *Barry et al.* [1996] applied this modified equation to study the propagation of small-amplitude oscillations in a coastal aquifer. The results showed that the damping rate of the oscillations propagating inland quickly reaches an asymptotic finite value as the forcing frequency on the boundary increases. In other words, the damping effects on a high-frequency oscillation are not overwhelming but rather bounded. This implies that with capillarity effects, the water table will fluctuate in response to high-frequency sea level oscillations, as observed in the field. We shall elaborate upon this mechanism in detail in the following section.

The shortcomings of using the Boussinesq equation to simulate coastal groundwater flow have been discussed by *Nielsen* [1990] and *Li et al.* [1996]. The main deficiency is the absence of seepage face dynamics. It is necessary to consider two-dimensional flow to incorporate such phenomena. *Li et al.* [1996] have developed a BEM (boundary element method) model for simulating tidal fluctuations of beach water tables. To model high-frequency oscillations, capillarity effects need to be included. We modify the kinematic boundary condition for the water table using an additional term following *Parlange and Brutsaert* [1987]. This condition accounts for mass transfer across the moving water table due to the capillarity effects.

In the present paper we first describe the conceptual and numerical models. We then present the results of some numerical tests on the model and compare them with the analytical predictions of *Barry et al.* [1996]. Finally, we show an example of simulating water table responses to wave run-up.

2. Conceptual and Numerical Models

Modified Kinematic Boundary Condition for the Beach Water Table

A typical configuration of the problem is illustrated schematically in Figure 1. Owing to boundary condition changes at the beach face during the wave cycle, the water table fluctuates. The kinematic boundary condition (kbc) of the water table is [e.g., *Bear*, 1972; *Liggett and Liu*, 1983]

$$n_e \frac{\partial \phi}{\partial t} = -\frac{K}{\cos \beta} \frac{\partial \phi}{\partial n} - q, \; z = \eta(x, t), \tag{1}$$

where n is the local coordinate on the boundary in the normal direction outward from the domain, $\partial\phi/\partial n$ is the potential gradient in the normal direction, n_e is the effective porosity of the porous medium, q is the rate of the local mass transfer across the water table, and β is the angle between the free surface and x axis (Figure 1). Variable definitions are collected in the notation list.

Mass conservation in the unsaturated zone above the water table requires [*Parlange and Brutsaert*, 1987]

$$\int_{\eta}^{\infty} \frac{\partial \theta}{\partial t} dz = n_e \frac{\partial \phi}{\partial t} + q, \tag{2}$$

where θ is the water content in the unsaturated zone. To determine the mass flux (q), the unsaturated flow equation (one-dimensional Richards equation) needs to be solved. *Parlange and Brutsaert* [1987] have obtained the following approximate expression for q:

$$q = -\frac{B}{K} \frac{\partial}{\partial t} \left(\int_{\eta}^{\infty} \frac{\partial \theta}{\partial t} dz \right), \tag{3}$$

where B is the thickness of the capillary fringe. Combining (1)–(3) gives the modified kbc for the water table, i.e.,

$$\frac{\partial \phi}{\partial t} = -\frac{K}{n_e \cos \beta} \frac{\partial \phi}{\partial n} - \frac{B}{n_e \cos \beta} \frac{\partial}{\partial t} \left(\frac{\partial \phi}{\partial n} \right), \; z = \eta(x, t). \tag{4}$$

To interpret the physical meaning of (4), we choose the period and amplitude of the sea level oscillations as the timescale and length scale to nondimensionalize the equation; thus

$$\frac{\partial \phi^*}{\partial t^*} = -\left[\frac{KT}{An_e \cos \beta} \frac{\partial \phi^*}{\partial n^*} \right] - \left[\frac{B}{An_e \cos \beta} \frac{\partial}{\partial t^*} \left(\frac{\partial \phi^*}{\partial n^*} \right) \right] \tag{5}$$

where $(\,)^*$ are the nondimensional variables. From (5), we can see that there are two mechanisms causing the water table fluctuations: horizontal mass transport and local mass transfer across the water table.

Two Mechanisms of Beach Water Table Fluctuations in Response to Sea Level Oscillations

The first mechanism appears in (5) as the first term on the right-hand side. It is essentially due to a horizontal mass transport process which results from the boundary condition changes at the beach face. This is illustrated in Figure 2. The mass flux across the water table, $K(\partial\phi/\partial n)$, results from the net horizontal water movement and causes the water table elevation changes (i.e., $\Delta\eta_1$). In other words, the water table fluctuations are induced by the landward propagation of the sea level oscillation. As the oscillation propagates inland, the amplitude is attenuated and the phase changes (i.e., there are time lags among the local water table fluctuations measured at different locations). Obviously, if the beach sand has a high hydraulic conductivity, the damping effects and phase shifts are small. On the other hand, for a given beach, high-frequency oscillations are subject to large damping and phase modification.

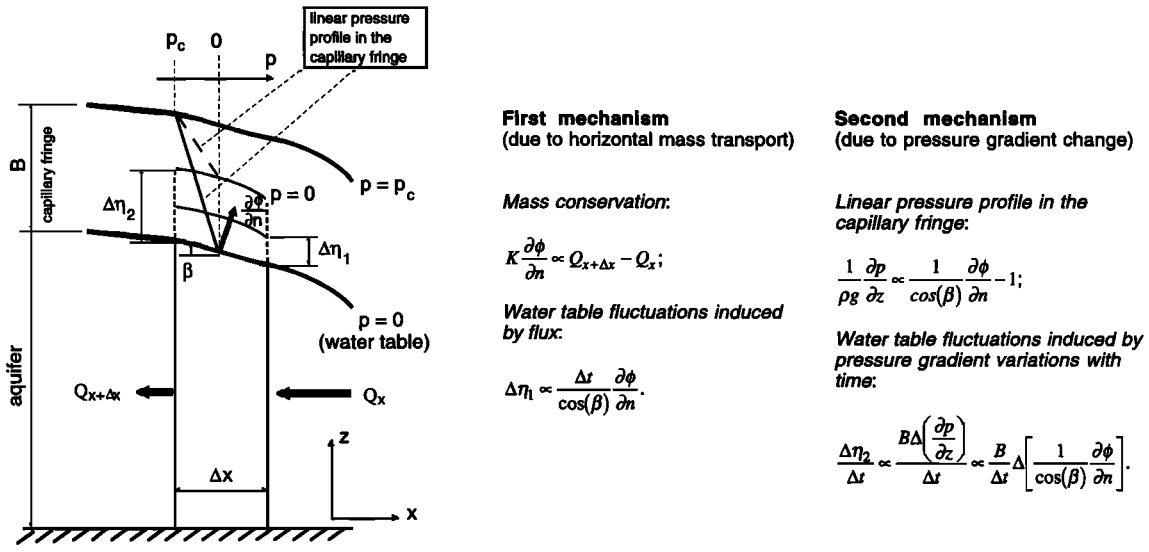

Figure 2. Schematic diagram of the horizontal mass movement, pressure gradient change, and water table fluctuation in a small cross segment (Δx) over time Δt. It shows the two mechanisms controlling coastal groundwater table fluctuations.

The second mechanism appears in (5) as the second term on the right-hand side and is due to a local mass transfer across the water table. This mass transfer process is a result of the pressure gradient changes at the water table. As shown in Figure 2, the vertical pressure gradient inside the capillary fringe under the assumption of a linear pressure profile is constant and is related to the normal potential gradient at the water table as

$$\frac{1}{\rho g}\frac{\partial p}{\partial z} = \frac{1}{\cos\beta}\frac{\partial\phi}{\partial n} - 1. \tag{6}$$

As the water table fluctuates, the pressure at the top boundary of the capillary fringe remains almost unchanged (i.e., p_c in Figure 2 is constant). This is because pressure adjustment above the capillary fringe relies on unsaturated flow and is a slow process compared with water table fluctuations, particularly at high frequencies. This might not be true for very low frequency water table fluctuations. However, we will see in later discussion that the second mechanism is not important in that case, and thus the validity of this assumption is irrelevant. Given that the pressure is constant at the top boundary of the capillary fringe, any pressure gradient variations with time inside the capillary fringe will result in instantaneous changes of the zero-pressure location (i.e., the water table), as indicated in Figure 2. In other words, the water table fluctuates in response to the pressure gradient change ($\Delta\eta_2$). The associated local mass transfer rate is represented by the second term on the right-hand side of (5). Note that this local mass transfer is an apparent process which does not reflect appreciable water movement. The water table (i.e., the phreatic surface) can fluctuate within the capillary fringe without much water movement since the water saturation inside the capillary fringe is close to unity. It is clear that under this mechanism the water table responses to the sea level oscillations are simultaneous; that is, there is no phase shift between the local water table fluctuations. However, the amplitude of the fluctuations is also damped inland.

These two mechanisms compete with each other. If the period T of the oscillations and the conductivity of the sand are both large, the first mechanism is dominant and capillarity effects are negligible. However, with high-frequency oscillations and a large capillary fringe, capillarity effects are dominant and the water table will respond according to the second mechanism. The absence of the second mechanism in numerical models causes the failure of these models to predict the water table response to high-frequency sea level oscillations.

To recap, water table fluctuations behave differently depending on the frequency of the sea level oscillations. For tidal sea level oscillations, there exist phase shifts in the water table fluctuations because the first mechanism dominates. This has been demonstrated in field observations by *Nielsen* [1990]. In that study, measurements of tidal groundwater table fluctuations were taken at five different horizontal locations (three of them are shown in Figure 3a). The results clearly show that there exists a time lag in the water table fluctuations. For high-frequency sea level oscillations due to wave run-up, the second mechanism is dominant, and thus the water table response is expected to be simultaneous, as observed in the *Waddell* [1976] field study. Two water table measurement wells were located 5 and 6 m landward of the mean shoreline, both outside the swash zone. The water tables at these two locations were found to respond to wave run-up simultaneously (Figure 3b). Note that a time lag of about 3 s existed between the swash oscillation measured 3 m landward of the mean shoreline and the beach water table fluctuations. This is due to the nonuniform transformation of waves on the beach. The swash oscillations on the beach face are not uniform, and so neither are the resulting pressure fluctuations on the beach face (the seaward boundary conditions for the groundwater flow). However, we will show later from the numerical results that the phase of the water table fluctuations is solely determined by that of the shoreline oscillations. In both cases, the frequencies of the water table fluctuations correspond well to those of the tide and wave run-up (Figure 3).

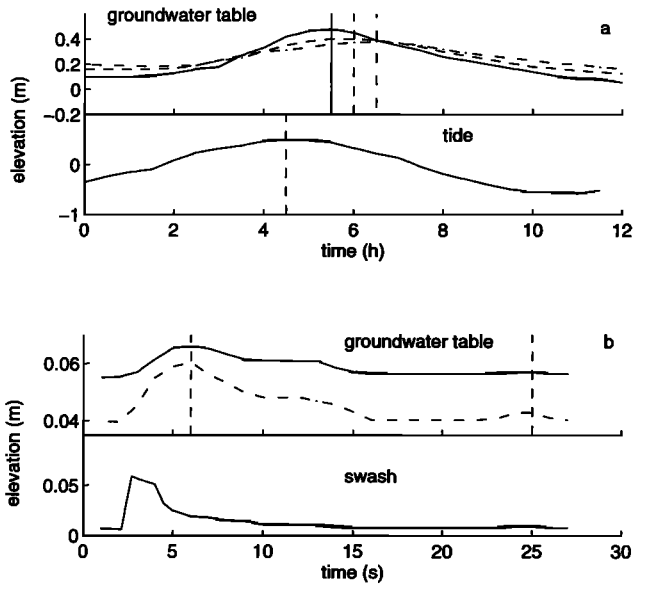

Figure 3. Field observations. (a) Tidal groundwater table fluctuations [*Nielsen*, 1990]. Solid, dashed, and dash-dotted lines are water table elevations at locations 6.6, 9.1, and 11.6 m landward, respectively, of the mean shoreline. The vertical lines, indicating the peaks of these water table elevations, show the time lag that exists in the water table fluctuations. The tide is shown in the bottom portion of the plot. (b) Water table fluctuations due to wave run-up [*Waddell*, 1976]. Two vertical lines show that the peaks occur at the same time in the two water table signals (5 and 6 m landward of the mean shoreline), indicating that no phase shift exists in the water table fluctuations. The swash oscillation measured 3 m landward of the mean shoreline is shown in the lower portion of the plot.

Relative Importance of Capillarity Effects

To quantify the competition between the two mechanisms, we define a nondimensional number called the CAR (coastal aquifer response) number, N_{CAR}, which is simply the ratio of the magnitude of the first term to that of the second term on the right-hand side of (5):

$$N_{CAR} = \frac{K}{B\omega}, \tag{7}$$

where ω $(2\pi/T)$ is the frequency of the boundary oscillations. Clearly, the first mechanism is dominant if N_{CAR} is large, while the second mechanism prevails for small N_{CAR}. A critical value of N_{CAR} for transition between the two mechanisms can be determined from experimental data, numerical results, or analytical solutions. For example, according to *Barry et al.* [1996], the critical value of N_{CAR} is $\sqrt{3}$ for a small-amplitude oscillation in a semi-infinite rectangular domain.

The CAR number can also be thought of in terms of the response time of the capillary fringe ($T_f = B/K$) and the timescale for water table fluctuations ($T_w = 1/\omega$), i.e., $N_{CAR} = T_w/T_f$. This offers another insight into the second mechanism. For a high-frequency sea level oscillation (N_{CAR} is small), the timescale of the water table fluctuation is much shorter than the response time of the capillary fringe. Therefore the capillary fringe will not be able to adjust itself to reach another equilibrium state as the water table rises or falls; consequently, the aquifer gains water from the fringe as the water table rises and loses water as the water table falls. Such water exchange between the capillary fringe and aquifer enhances the water table fluctuations.

Modeling Two-Dimensional Groundwater Flow Using a BEM Model

The modified kbc (4) is incorporated into a BEM (boundary element method) model enabling the simulation of high-frequency water table fluctuations due to wave run-up. The BEM model solves the two-dimensional Laplace equation for the potential in the aquifer with moving boundary conditions at the beach face and free surface boundary conditions at the water table. The details of the BEM model have been described by *Li et al.* [1996].

Shallow Water Equations for Modeling Wave Run-Up on the Beach

The depth-averaged shallow water equations (SWE) are used to model wave run-up on the beach. The applicability of SWE for wave run-up on a beach has been discussed by *Peregrine* [1972]. The governing equations consist of the continuity and momentum equations [e.g., *Hibberd and Peregrine*, 1979; *Kobayashi et al.*, 1987]:

$$\frac{\partial h}{\partial t} + \frac{\partial}{\partial x}(hu) = 0, \tag{8}$$

$$\frac{\partial}{\partial t}(hu) + \frac{\partial}{\partial x}(hu^2 + \tfrac{1}{2}gh^2) = -\tan(\gamma)gh, \tag{9}$$

where h and u are the depth and flow velocity of the seawater, respectively, (Figure 1), g is the magnitude of the gravitational acceleration, and γ is the beach angle.

Equations (8) and (9) can be solved using the numerical scheme developed by *Hibberd and Peregrine* [1979]. The solutions give the sea surface elevations at each time step, which are then used to determine the boundary conditions at the beach face for the BEM model. Thus, by solving both the Laplace equation for the coastal groundwater flow and the SWE for the wave motion, we can study the response of the water table to the sea level oscillations due to wave run-up.

3. Numerical Tests and Comparison With Analytical Predictions of *Barry et al.* [1996]

Analytical Solution for Small-Amplitude Oscillations

As mentioned previously, *Barry et al.* [1996] have derived an approximate analytical solution for small-amplitude oscillations based on the modified one-dimensional Boussinesq equation, i.e., including capillarity effects:

$$n_e \frac{\partial \eta}{\partial t} = K \frac{\partial}{\partial x}\left(\eta \frac{\partial \eta}{\partial x}\right) + B \frac{\partial^2}{\partial t \partial x}\left(\eta \frac{\partial \eta}{\partial x}\right). \tag{10}$$

They considered a small-amplitude oscillations at the vertical beach face as described by

$$\eta(0, t) = D[1 + \varepsilon \cos(\omega t)], \tag{11}$$

where D is the average thickness of the aquifer, ε is the ratio of the oscillation amplitude to D, and ω is the frequency of the oscillation. It is assumed that the seepage face is nonexistent. A series solution up to the second order in ε was obtained. For small-amplitude oscillations, the first-order solution dominates, and the water table fluctuations can be approximated by

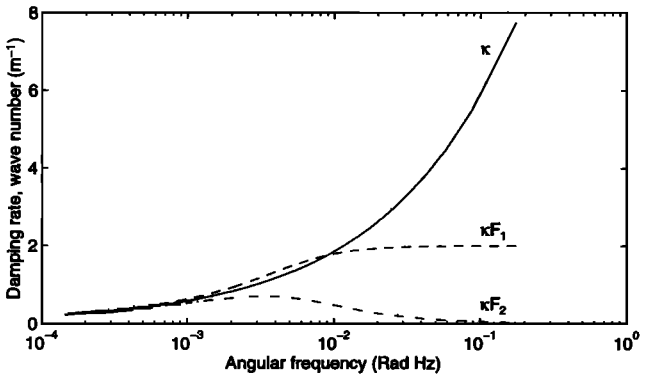

Figure 4. Analytical predictions of the oscillation damping rate and wave number varying with ω. The solid line is the damping rate without capillarity effects (wave number equals the damping rate). Dashed and dash-dotted lines are the damping rates and wave numbers with capillarity effects, respectively.

$$\eta(x, t) = D[1 + \varepsilon \exp(-x\kappa F_1) \cos(\omega t - x\kappa F_2)], \quad (12)$$

where

$$\kappa = \sqrt{\frac{n_e \omega}{2KD}},$$

$$F_1 = \sqrt{\frac{N_{CAR}}{\sqrt{1 + N_{CAR}^2}} + \frac{N_{CAR}}{1 + N_{CAR}^2}},$$

$$F_2 = \sqrt{\frac{N_{CAR}}{\sqrt{1 + N_{CAR}^2}} - \frac{N_{CAR}}{1 + N_{CAR}^2}}.$$

The term κF_1 in (12) is the damping rate, and κF_2 is the wave number which determines the phase change as the oscillation propagates inland. For $B = 0$, we have $F_1 = F_2 = 1$, and the above solution reduces to that for the oscillation propagation without capillarity effects [*Parlange et al.*, 1984; *Nielsen*, 1990]. It is clear that in this case, high-frequency oscillations will be damped quickly because the damping rate (κ) increases with the frequency ω. When there is a capillary fringe, B is nonzero, and (12) shows that the damping rate is modified by a factor F_1. The relation between the damping rate (κF_1) and ω is thus changed (Figure 4) (the values of D, K, B and n_e are taken to be 1 m, 5.8×10^{-4} m s^{-1}, 0.1 m, and 0.4, respectively). The damping rate increases with ω initially and then quickly goes to an asymptote, $\sqrt{n_e/BD}$ (dashed line in Figure 4). This implies that the damping does not overwhelm the high-frequency oscillations, and thus high-frequency water table responses will be observed.

Another feature of the water table fluctuations with capillarity effects is that as the frequency of the oscillation increases, the phase shift of the water table responses first increases to a maximum level and then decreases to zero (Figure 4, dash-dotted liens). The initial increase reflects the dominant effect of the first mechanism of water table fluctuations. At the maximum level the first and second mechanisms are in balance and N_{CAR} reaches the critical level, the value of which is $\sqrt{3}$ according to (12). As ω continues to increase, the second mechanism becomes dominant and phase shift vanishes. In summary, the behavior of the water table fluctuation predicted by the analytical solution is in accordance with the mechanistic behavior presented above.

Numerical Tests

Numerical tests using the BEM model (developed by *Li et al.* [1996]) with the modified kinematic boundary condition were carried out to compare with the above analytical predictions. The simulations were conducted in a 10 m × 1 m domain. The hydraulic conductivity and porosity of the sand were set to be 5.8×10^{-4} m s^{-1} and 0.4, respectively, both values being representative of beach sand. The thickness of the capillary fringe is 0.1 m [*Bear*, 1972]. A small-amplitude oscillation was specified at the vertical beach face ($x = 10$ m), i.e., $z_s(t) = 1 + 0.04 \cos \omega t$ m. Simulations were conducted with and without capillarity effects. The purpose was to examine the water table fluctuations as responses to sea level oscillations with periods ranging from 10 s (typical swell wave period) to 12 hours (semidiurnal tide period).

As examples, we show the time series of water table responses to the sea level oscillations for the two extreme cases, with the oscillation periods equal to 10 s and 12 hours (N_{CAR} = 0.0092 and 39.8736, respectively). The results for $T = 10$ s are shown in Figure 5, while those for $T = 12$ hours are shown in Figure 6. A comparison of these two figures shows that the capillarity effects are very significant when the frequency of the oscillations is high and are negligible for low-frequency oscillations. This is obviously consistent with the mechanisms of water table fluctuations and the analytical predictions.

The propagation of the oscillations in the aquifer is shown in Figures 7 and 8, where we plot the local water table fluctuations at different horizontal locations: x = 9.3, 9.4, 9.5, 9.6, 9.7, 9.8, and 9.9 m subject to boundary oscillations at $x = 10$ m. In both high- and low-frequency cases, the oscillations were found to be damped as they propagate landward into the aquifer. While there is a time lag in the low-frequency oscillations, the high-frequency oscillations occur simultaneously.

From the results, we can distinguish the following features of the water table responses as predicted by the analytical solution of *Barry et al.* [1996]:

1. With capillarity effects, high-frequency sea level oscillations will induce water table fluctuations (Figures 5 and 7). The water table responses are simultaneous with the sea level oscillations, that is, there is no phase shift (Figure 7). This phenomenon does not appear without capillarity effects (Figures 5 and 7).
2. Capillarity effects are negligible for low-frequency oscillations (Figure 6).
3. For low-frequency oscillations the phase shift increases inland (Figure 8).
4. The frequency of water table fluctuations is equal to that of sea level oscillations in both high- and low-frequency cases (Figures 7 and 8).

Simulations were also conducted with the periods of sea level oscillations equal to 10, 8, 6, 4, 2, and 1 hours, and 1200, 600, 300, 60, 30, and 20 s. For each case we calculated the amplitudes and phase changes of the local water table fluctuations, from which the damping rate and wave number of the oscillations were estimated. The results were found to be in good agreement with the analytical solution (Figure 9). With capillarity effects, the damping rate was bounded by a finite value; the phase shift between water table fluctuations and sea level oscillations vanished as the frequency increased (Figure 9).

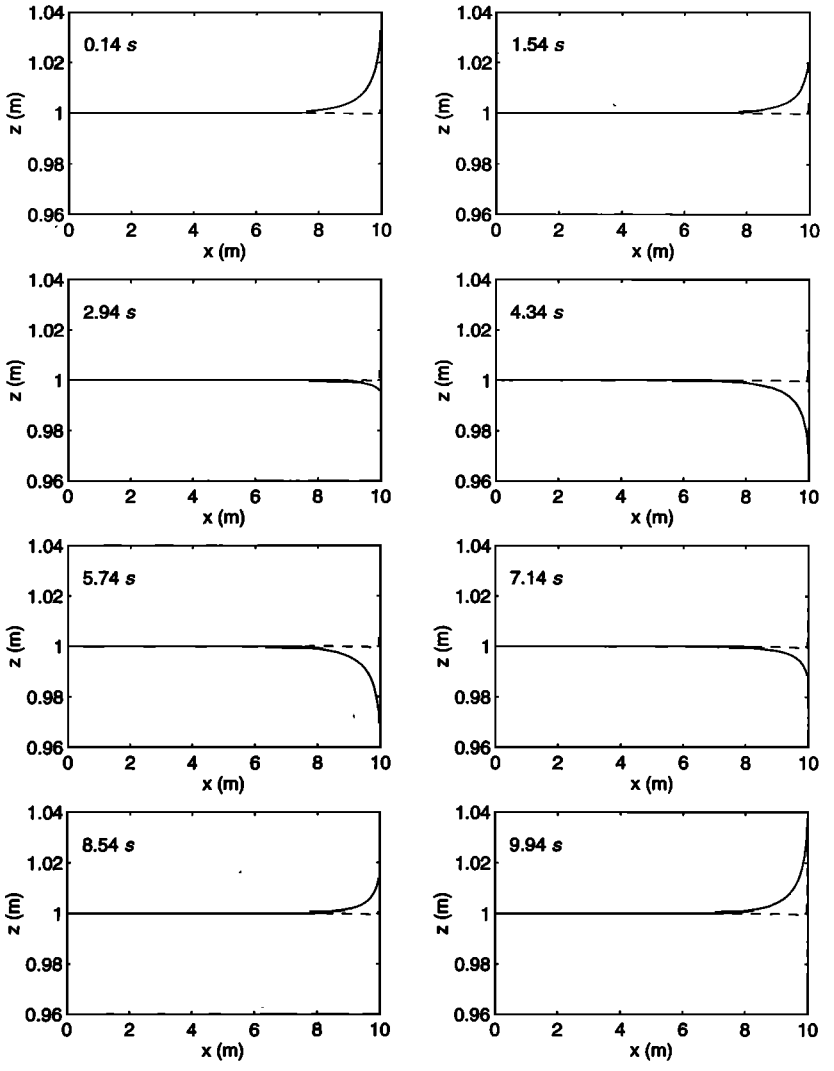

Figure 5. Water table fluctuations in response to high-frequency water level oscillations at the vertical right-side boundary. Solid lines are water table responses with capillarity effects, and dashed lines are those without capillarity effects.

Seepage Face Dynamics

For small-amplitude oscillations, seepage face formation at the oscillating boundary is negligible. However, the dynamics of the seepage face becomes important when increased amplitude oscillations are considered. This is often the case on natural beaches. The extent of the seepage face is relatively large and varies with time. It is therefore important to look at the propagation of finite amplitude oscillations. The BEM model is capable of simulating seepage face dynamics [*Li et al.*, 1996].

Another set of simulations were carried out with increased amplitude oscillations specified at the vertical face, i.e., $\varepsilon = 0.4$. The results on the damping rate and phase shift of the oscillations were found to behave in the same manner as above. The comparison with the analytical predictions is also good, similar to that shown in Figure 9. The explanation for such good agreement is that the existence of the seepage face changes the boundary conditions at the beach face (i.e., equation (11) is no longer valid, and so neither is (12)), but it has little effect on the water table response. Therefore the damping rate and the phase change do not vary considerably.

To examine the capillarity effects on the seepage face, we plotted in Figure 10 the seepage face variations in both cases (i.e., with and without capillarity effects) for $T = 10$ s. The results indicate that with capillarity effects, the seepage face is reduced significantly. Such a reduction is another indication of the enhancement of water table response to high-frequency sea level oscillations as induced by capillarity effects.

4. Simulation of Water Table Fluctuations Due to Wave Run-Up

Thus far we have considered only a vertical beach face. We now proceed to the case of a sloping beach, to which the theory of *Barry et al.* [1996] does not apply. As mentioned previously, the SWE was used to simulate wave run-up on the beach. To solve the SWE, we need to define the boundary conditions along the beach. At the seaward boundary where values of u and h need to be determined for each time step, a periodically varying function (soliton-like) was specified for the advancing characteristic variable [*Hibberd and Peregrine*, 1979], i.e.,

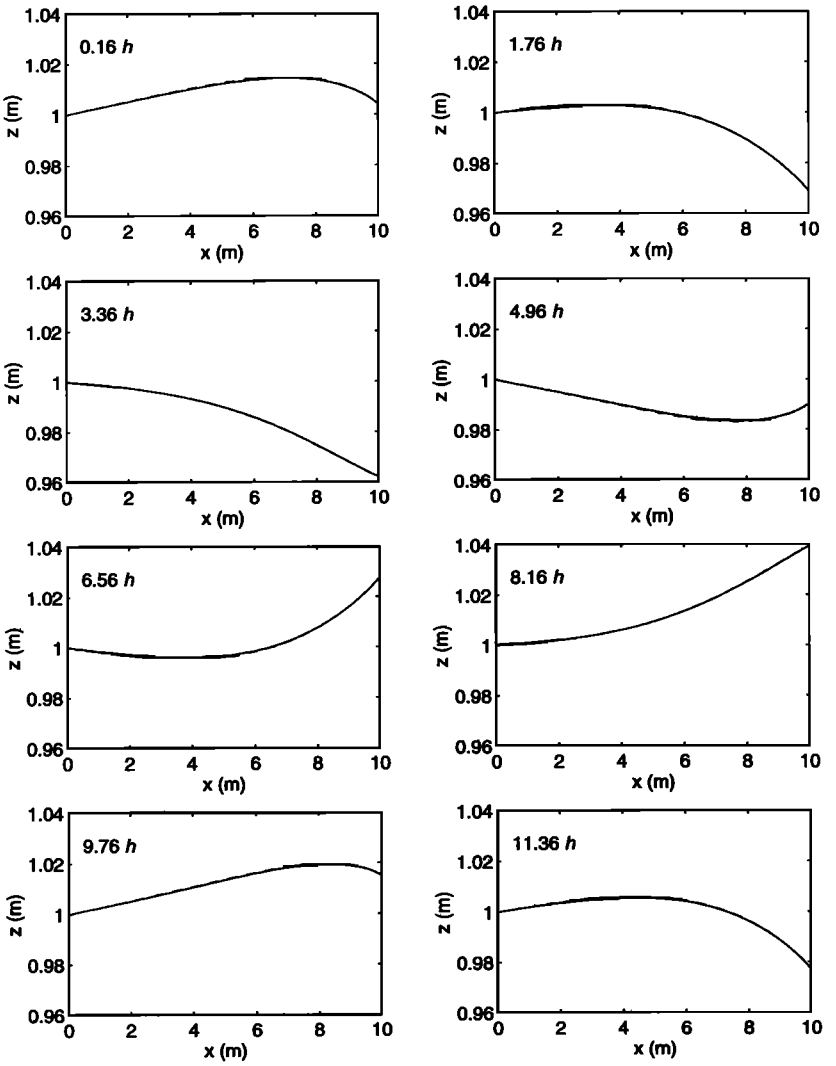

Figure 6. Water table fluctuations in response to low-frequency water level oscillations at the vertical right-side boundary. Solid lines are water table responses with capillarity effects, and dashed lines are those without capillarity effects.

$$\alpha_{ad} = 2\sqrt{gH_0} + \frac{\sqrt{gH_0}}{\{\cosh[t - \text{int}\ (t/T) \times T]\}^2}, \quad (13)$$

where $\alpha_{ad} = u + 2\sqrt{gh}$, H_0 is the still water level (Figure 1; it fluctuates with the tide in reality), T is the period for the variations of α_{ad}, and int ( ) is a function which returns the integer part of the variable. From the governing equations of the characteristic variables we can calculate the receding characteristic variable, which is defined as $\alpha_{rd} = -u + 2\sqrt{gh}$. The values of u and h at the seaward boundary can subsequently be determined from α_{ad} and α_{rd}. The landward boundary is the moving shoreline, the location and condition of which are determined by the procedures described by *Hibberd and Peregrine* [1979].

Once the sea level elevations which vary with the wave motion on the beach are known from the solutions of the SWE, the boundary conditions at the beach face for the groundwater flow are well defined. Thus the Laplace equation can be solved to give the water table elevations at each time step. It should be pointed out that although the Laplace equation does not contain any time differential term, the problem is transient because the boundary conditions are time varying.

The simulation domain is 20 m long at the impermeable base, while the beach slope is 0.1. The landward boundary condition for groundwater flow is prescribed by a constant head of 1 m. The hydraulic conductivity and porosity of the sand are 4×10^{-4} m s^{-1} and 0.4, respectively. The thickness of the capillary fringe is 0.1 m. The still water level (H_0) is taken to be 0.6 m above the base, and the period for the variations of α_{ad} (T) is 20 s. These parameter values are considered to be typical for some beach conditions and were chosen for the purpose of illustration.

Time Series of the Wave Run-Up and Water Table Response

The elevations of the sea level and water table from the simulations are plotted every 2 s over one wave cycle (Figure 11). The response of the water table to wave run-up is clearly evident. The local water table fluctuations at two horizontal locations ($x = 9$ and 10 m, both landward of the swash zone) are displayed in Figure 12, where the shoreline elevations and

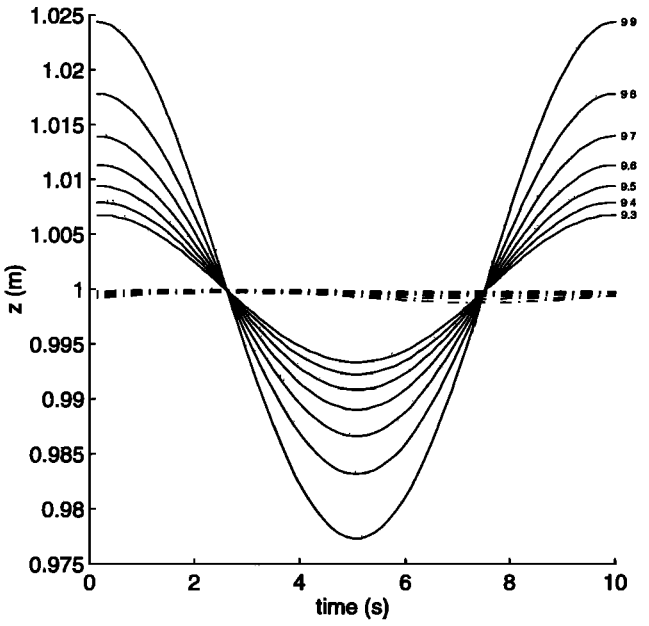

Figure 7. Local water table fluctuations due to high-frequency water level oscillations at the vertical right-side boundary. Solid lines are water table responses with capillarity effects, and dashed lines are those without capillarity effects.

the sea level oscillations at $x = 16$ m (inside the swash zone) are also plotted. The shoreline here refers to the intersection between the sea surface and the beach face (point S in Figure 1). By inspection, we see that the water table response occurs simultaneously with the shoreline movement. Although the wave-induced pressure fluctuations on the beach face were not uniform, this result indicated that the phase of the water table

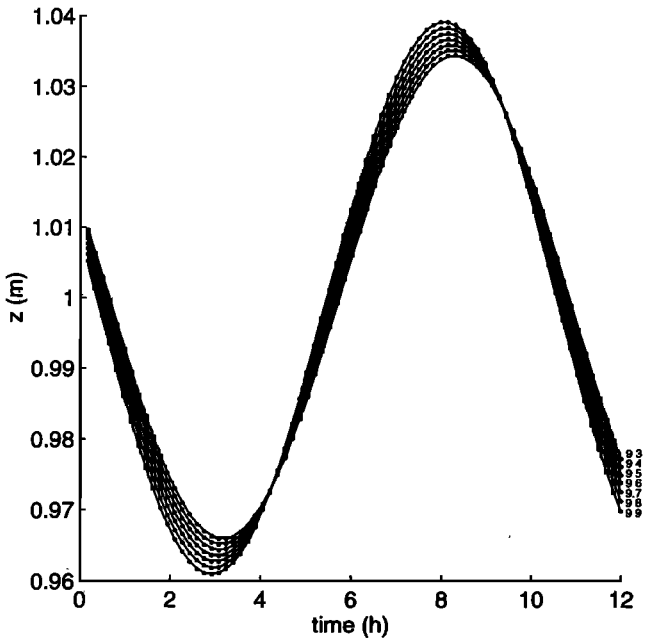

Figure 8. Local water table fluctuations due to low-frequency water level oscillations at the vertical right-side boundary. Solid lines are water table responses with capillarity effects, and dashed lines (overlapping the solid lines) are those without capillarity effects.

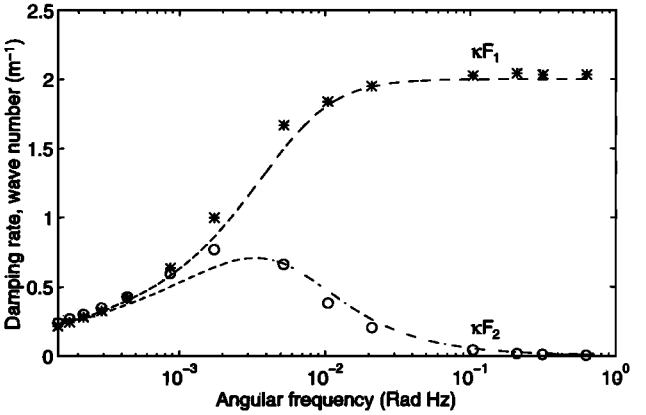

Figure 9. Comparison of the damping rate and wave number with analytical predictions (small amplitude). Stars and circles are the numerical results of the damping rate and wave number, respectively. Dashed and dash-dotted lines are the analytical predictions of the damping rate and wave number, respectively.

fluctuations is mainly determined by that of the shoreline oscillations. The swash oscillations at $x = 16$ m, on the other hand, were about 7 s ahead the water table fluctuations, similar to the field observations as shown in Figure 3b.

Also shown in Figures 11 and 12 are the water table elevations from the comparison simulations with no capillarity effects. While high-frequency water table fluctuations are evident in the results with capillarity effects, no fluctuations can be observed at the water table in the case without capillarity effects.

The time-averaged (over the swash cycle) locations of the fluctuating water tables are higher than the ones which are obtained from the simulations of tidal groundwater fluctuations, i.e., without wave run-up (Figure 13). The differences between them obviously result from the propagation of the sea level oscillations due to wave run-up. Such a setup of the water table has been observed in the field and has important effects on wave motion on the beach [*Aseervatham et al.*, 1993; *Turner*, 1993].

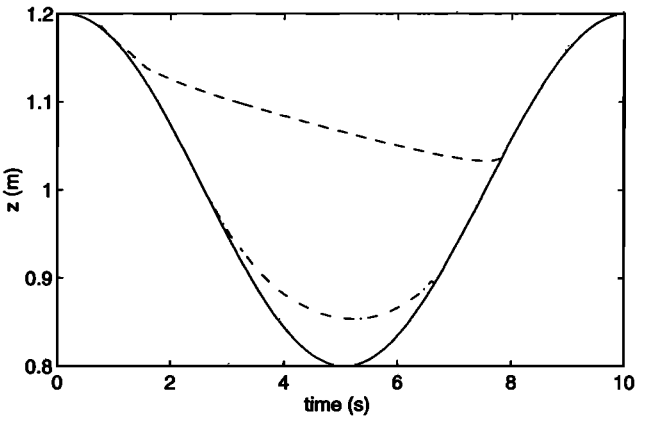

Figure 10. Seepage face reduction due to capillarity effects. The solid line represents the water level oscillations. Dash-dotted and dashed lines are the elevations of the exit point with and without capillarity effects, respectively.

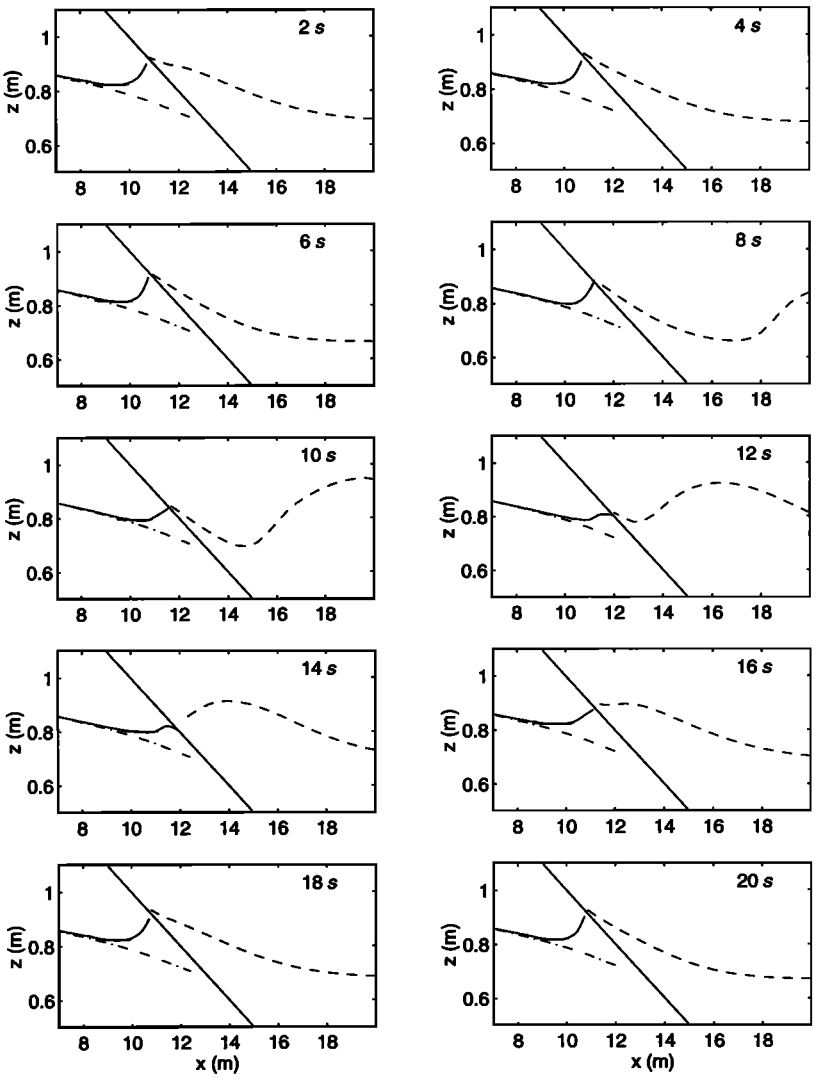

Figure 11. Water table responses to wave run-up on the beach. The dashed lines represent sea level oscillations, the solid lines show the water table response with capillarity effects, and the dash-dotted lines show the water table response without capillarity effects.

Spectral Analysis

Following *Hegge and Masselink* [1991], we applied the Fourier transform technique to analyze the above numerical data. Power spectral densities for water table fluctuations at $x = 10$ m and shoreline oscillations were computed. The phase shift and coherence between them were also computed. The results are shown in Figure 14.

The peaks of the power spectral densities for wave signals and water table fluctuations both occur at $\omega = 0.31$ rad Hz ($f = 0.05$ Hz), which corresponds to the variation period specified for α_{ad} in the simulations. This indicates that water table fluctuations are induced by wave run-up. Such a correlation is confirmed by the high coherence between the two time series at the peak frequency (Figure 14d). The results also show that almost no phase shifts exist between the water table fluctuations and the shoreline movement (Figure 14c). This confirmed the previous observation on the simulation results, that is, the water table fluctuations were simultaneous with the shoreline movement.

In summary, a high-frequency water table response to wave

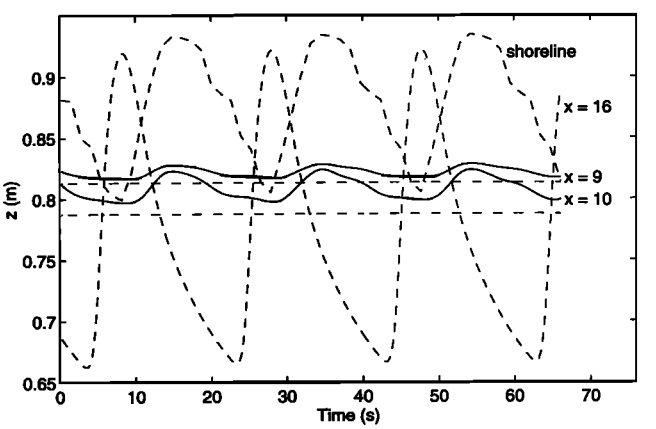

Figure 12. Local water table response and sea level oscillations. The dashed lines represent the shoreline elevations and sea level elevations at $x = 16$ m. The solid lines show the water table response with capillarity effects at $x = 10$ m and $x = 9$ m. The dash-dotted lines represent the water table responses without capillarity effects at $x = 10$ m and $x = 9$ m.

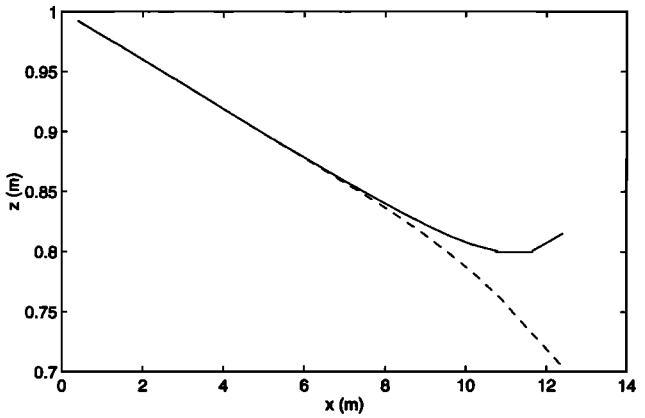

Figure 13. Water table setup due to wave motion. The solid line is the time-averaged (over a wave period) location of the water table fluctuating with wave run-up. The dashed lines show the water table without wave influence.

run-up has been observed in the simulation, and it has the same features as those shown in the previous sections: The oscillations are standing wave-like with the amplitude damped inland.

Uncertainties are present in the field observations [*Waddell*, 1976]. For example, the seaward boundary conditions for the wave motion and the landward boundary conditions for the groundwater flow are unknown. With both boundary conditions missing we have not attempted to simulate the field data using the model at this stage. However, field studies have shown high-frequency water table fluctuations in response to the wave motion (Figure 3b). The features of these field observations are comparable with the numerical results, in particular, the instantaneous characteristics of the water table responses (Figure 3b) [*Waddell*, 1976].

5. Conclusions

The coastal groundwater table fluctuates in response to high-frequency sea level oscillations due to wave run-up. These high-frequency water table fluctuations significantly affect the infiltration/exfiltration process at the beach face and hence beach stability. They also largely control the interstitial oxygenation processes and biological reactions in the beach ecosystem. Accurate representation of high-frequency beach water table fluctuations is therefore of importance in modeling the interaction between coastal groundwater and seawater.

Previous models considered only saturated flow. The absence of capillarity effects causes the failure of the models in predicting high-frequency water table responses to wave run-up. In fact, the simulated water table will not respond to high-frequency sea level oscillations due to the high damping effects.

In this paper we have developed a modified kinematic boundary condition for the water table, which takes into account the capillarity effects. The new kbc was incorporated into a BEM model. The model was then applied to simulate water table response to high-frequency sea level oscillations in a rectangular domain, and the results were found to be consistent with the analytical predictions of *Barry et al.* [1996]. We also used the model to simulate the water table response to wave run-up at a sloping beach. The simulated water table behavior was similar to that observed in the field [*Waddell*, 1976]. Although the wave-induced pressure fluctuations on the beach face were not uniform, the phase of the water table response was found to be determined solely by the shoreline movement.

On the basis of results presented in the paper, we conclude that capillarity effects provide a mechanism for high-frequency water table fluctuations as responses to wave run-up. Second,

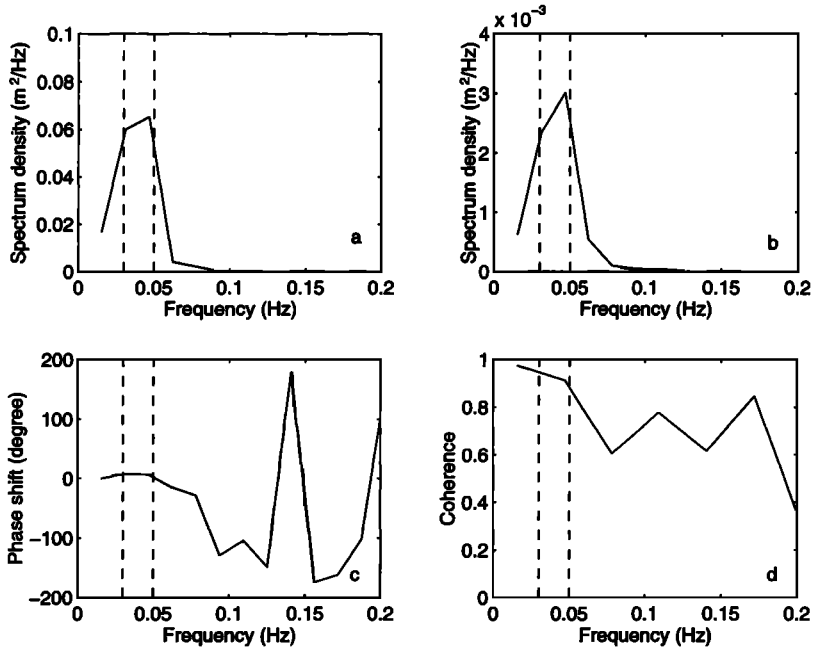

Figure 14. Spectral analysis of the water table response to wave run-up on the beach (numerical simulation). (a) Power spectrum of wave run-up (shoreline movement). (b) Power spectrum of the water table response at $x = 10$ m. (c) Phase shift and (d) coherence between shoreline oscillations and water table responses. The vertical dashed lines indicate the frequency range where most of the oscillation energy is accumulated.

the modified kbc for the water table is a physically reasonable representation of such effects and can be easily incorporated into any two-dimensional model (such as the BEM model used in the present study) for simulating high-frequency beach water table fluctuations.

Finally, we would like to point out that the reverse Wieringermeer effect has not been discussed in the present paper. This effect is partly responsible for high-frequency water table fluctuations underneath the swash zone [*Hegge and Masselink*, 1991], a zone not considered here. The field observations [*Waddell*, 1976] and the numerical simulations we have presented are both concerned with water table fluctuations landward of the swash zone. However, the inclusion of this effect in the model should be considered in future work. Also, direct simulation of the field data by the model is desirable in later investigations.

Notation

A amplitude of the oscillation $[L]$.
B thickness of the capillary fringe $[L]$.
D averaged thickness of the aquifer $[L]$.
F_1 modification factor of the damping rate.
F_2 modification factor of the wave number.
f frequency of the oscillation, $1/T$ [Hz].
h seawater depth $[L]$.
K hydraulic conductivity $[L\ T^{-1}]$.
l length of the baseline $[L]$.
n local coordinate in the normal direction on the boundary $[L]$.
n_e effective porosity.
p pressure $[M\ L^{-1}\ T^{-2}]$.
p_c capillary pressure at the top boundary of the capillary fringe $[M\ L^{-1}\ T^{-2}]$.
Q horizontal net flux $[L^2\ T^{-1}]$.
q local mass transfer rate across the water table $[L\ T^{-1}]$.
T period of the oscillation $[T]$.
t time $[T]$.
u velocity of seawater $[L\ T^{-1}]$.
x horizontal coordinate $[L]$.
z vertical coordinate $[L]$.
z_D elevation of the exit point $[L]$.
z_s sea level elevation $[L]$.
α_{ad} advancing characteristic variable, $u + 2\sqrt{hg}$ $[L\ T^{-1}]$.
α_{rd} receding characteristic variable, $-u + 2\sqrt{gh}$ $[L\ T^{-1}]$.
θ water content.
ϕ potential head, $p/\rho g) + z$ $[L]$.
ρ water density $[M\ L^{-3}]$.
β angle between the free surface and the horizontal axis [rad].
γ beach angle [rad].
ω oscillation frequency [rad T^{-1}].
η water table elevation $[L]$.
κ damping rate, wave number $[L^{-1}]$.
$\partial p/\partial z$ vertical pressure gradient $[M\ L^{-2}\ T^{-2}]$.
$\Delta\eta_1$ water table fluctuation due to horizontal mass transport $[L]$.
$\Delta\eta_2$ water table fluctuation due to pressure gradient change $[L]$.

Acknowledgments. We are grateful to G. Masselink for his valuable comments on the paper. The first author thanks the University of Western Australia for financial support under University Fee-Waiver Scholarships and University Postgraduate Awards (International Students). This is University of Western Australia Centre for Water Research reference ED-1119LL.

References

Aseervatham, A. M., H. Y. Kang, and P. Nielsen, Groundwater movement in beach water tables, in *Proceedings of the 11th Australasian Conference on Coastal and Ocean Engineering*, pp. 589–594, Inst. of Eng., Barton, Australia, 1993.

Barry, D. A., S. J. Barry, and J.-Y. Parlange, Capillarity correction to periodic solutions of the shallow flow approximation, in *Mixing in Estuaries and Coastal Seas*, *Coastal Estuarine Stud.*, vol. 50, edited by C. B. Pattiaratchi, pp. 496–510, AGU, Washington, D. C., 1996.

Bear, J., *Dynamics of Fluids in Porous Media*, Elsevier, New York, 1972.

Duncan, J. R., The effects of water table and tide cycle on swash-backwash sediment distribution and beach profile development, *Mar. Geol.*, *2*, 186–197, 1964.

Grant, U. S., Influence of the water table on beach aggradation and degradation, *J. Mar. Res.*, *7*, 655–660, 1948.

Hegge, B. J., and G. Masselink, Groundwater-table responses to wave run-up: An experimental study from Western Australia, *J. Coastal Res.*, *7*, 623–634, 1991.

Hibberd, S., and D. H. Peregrine, Surf and run-up on a beach: A uniform bore, *J. Fluid Mech.*, *95*, 323–345, 1979.

Kobayashi, N., K. O. Ashwini, and I. Roy, Wave reflection and run-up on rough slopes, *J. Waterw. Port Coastal Ocean Eng.*, *113*, 282–298, 1987.

Lanyon, J. A., I. G. Eliot, and D. J. Clarke, Groundwater-level variations during semidiurnal spring tidal cycles on a sandy beach, *Aust. J. Mar. Freshwater Res.*, *33*, 377–400, 1982.

Li, L., D. A. Barry, and C. B. Pattiaratchi, Numerical modelling of tide-induced beach water table fluctuations, *Coastal Eng.*, in press, 1997.

Liggett, J. A., and P.L.-F. Liu, *The Boundary Integral Equation Method for Porous Media Flow*, Allen and Unwin, Winchester, Mass., 1983.

McLachlan, A., Intertidal zonation of macrofauna and stratification of meiofauna on high energy sandy beaches in the Eastern Cape, South Africa, *Trans. R. Soc. S. Afr.*, *44*, 213–223, 1989.

Nielsen, P., Tidal dynamics of the water table in beaches, *Water Resour. Res.*, *26*, 2127–2134, 1990.

Parlange, J.-Y., F. Stagnitti, J. L. Starr, and R. D. Braddock, Free-surface flow in porous media and periodic solution of the shallow-flow approximation, *J. Hydrol.*, *70*, 251–263, 1984.

Parlange, J.-Y., and W. Brutsaert, A capillary correction for free surface flow of groundwater, *Water Resour. Res.*, *23*, 805–808, 1987.

Peregrine, D. H., Equations for water waves and the approximations behind them, *Waves on Beaches and Resulting Sediment Transport*, edited by R. E. Meyer, Academic, San Diego, Calif., 1972.

Turner, I., The total water content of sandy beaches, *J. Coastal Res.*, *15*, 11–26, 1993.

Waddell, E., Swash-groundwater-beach profile interactions, *SEPM Spec. Publ.*, *24*, 115–125, 1976.

D. A. Barry and C. B. Pattiaratchi, Department of Environmental Engineering, University of Western Australia, Nedlands, Western Australia 6907. (e-mail: barry@cwr.uwa.edu.au; pattiara@cwr.uwa.edu.au)

L. Li, School of Engineering and Technology, Deakin University, Geelong, Victoria 3217, Australia. (e-mail: lingli@deakin.edu.au)

J.-Y. Parlange, Department of Agricultural and Biological Engineering, Cornell University, Ithaca, NY 14853-5701. (e-mail: jp58@cornell.edu)

(Received May 28, 1996; revised November 22, 1996; accepted December 17, 1996.)